Sustainable Energy & Fuels

ROYAL SOCIETY OF CHEMISTRY

PAPER

View Article Online
View Journal | View Issue

Cite this: *Sustainable Energy Fuels*, 2020, **4**, 2760

Improving the capacity and cycling-stability of Lithium–sulfur batteries using self-healing binders containing dynamic disulfide bonds†

Lei Duan,‡ Weihua Kong,‡ Wen Yan, Cheng-Hui Li, * Zhong Jin * and Jing-Lin Zuo *

Lithium–sulfur batteries, which can be applied for portable electronic devices with longer endurance, have received tremendous attention because of their high theoretical capacity and high energy density. However, both electrode volume variation and serious shuttling effects during the charge/discharge process limit the promotion of lithium–sulfur batteries. In this work, a novel self-healing poly(dimethylsiloxane) polymer with dynamic disulfide bonds (2S-PDMS) was designed as a binder for sulfur electrodes. The disulfide bonds in 2S-PDMS molecules can reversibly break and form, facilitating the conversion of polysulfides, as evidenced from both experimental and calculated results. In addition, 2S-PDMS binders with a remarkable self-healing ability and flexibility can keep the sulfur cathode integrated without cracks or damage. Consequently, the 2S-PDMS-based cathode exhibits both high capacity and excellent cycling stability, showing a specific capacity of 545.7 mA h g^{-1} at 2.0C after 400 cycles (79.6% capacity retention). Moreover, soft-packed Li–S batteries with a high sulfur loading of 6.6 mg cm^{-2} deliver a high areal capacity of 4.54 mA h cm^{-2} after 50 cycles, which verifies the good flexibility and stability of the 2S-PDMS-based cathode.

Received 26th February 2020
Accepted 30th March 2020

DOI: 10.1039/d0se00309c

rsc.li/sustainable-energy

Introduction

Lithium–sulfur (Li–S) batteries have been widely recognized as one of the most promising systems for next-generation energy storage devices due to their high theoretical capacity (up to 1675 mA h g^{-1}) and energy density (up to 2600 Wh kg^{-1}).[1–5] Moreover, sulfur is an inexpensive and environmentally friendly material, which benefits the commercial applications of Li–S batteries. However, Li–S batteries still have some serious problems that limit their development, such as low sulfur utilization, low coulombic efficiency, fast capacity fade and poor cycle life. These problems mainly arise from the poor electrical conductivity of sulfur, the large volume changes during the charge/discharge process, and the dissolution/diffusion of lithium polysulfides in electrolytes (shuttling effect).

So far, many strategies have been employed to solve these problems. The low conductivity of sulfur can be largely improved by incorporating sulfur into conductive matrices, such as carbonaceous materials,[6–11] conductive polymers,[12,13] and metallic compounds.[14] Porous or hollow cathode host materials were used to physically confine polysulfides and avoid large volume expansion.[15,16] In order to suppress the shuttling effect, researchers added polysulfide adsorbing/trapping agents into the electrodes to function as polysulfide reservoirs,[17,18] or introduced interlayers/separators between the cathode and the separator to prevent the migration of polysulfides.[19–21] Through these efforts, the performance of Li–S batteries has been improved obviously. However, the extra introduction of conductive matrices, separating interlayers, porous hosts and polysulfide absorbents would decrease the sulfur content of the sulfur electrode, finally influencing the whole energy density.

Developing functional polymer binders would be a better choice to improve the performance of Li–S batteries in a facile and economic manner. In lithium batteries, polymer binders are indispensable components which act as the physical adhesive to enhance the electrical contact between active materials and conductive agents and then to bond the active materials on the current collector. Therefore, modification of polymer binders would not significantly change the sulfur content of sulfur electrodes. The commercial binder polyvinylidene fluoride (PVDF) has poor elasticity and cannot impede the diffusion of polysulfide anions, thus exhibiting a poor electrochemical performance as binders in Li–S batteries.[22,23] In the past decade, various advanced polymer binders have been reported. Ductile polymers and polyelectrolyte binders have been reported to

State Key Laboratory of Coordination Chemistry, Key Laboratory of Mesoscopic Chemistry of MOE, Jiangsu Key Laboratory of Advanced Organic Materials, School of Chemistry and Chemical Engineering, Collaborative Innovation Center of Advanced Microstructures, Nanjing University, Nanjing 210023, P. R. China. E-mail: chli@nju.edu.cn; zhongjin@nju.edu.cn; zuojl@nju.edu.cn

† Electronic supplementary information (ESI) available. See DOI: 10.1039/d0se00309c

‡ These authors contributed equally to this work.

improve the performance of sulfur cathodes by sustaining volume expansion or regulating lithium-ion transport.[24–28] By utilizing self-healing binders, the resulting electrodes can autonomously repair the cracks formed by the volume variation during charging and discharging.[29] Despite these advances, challenges still exist on how to suppress the shuttle effect and improve sulfur utilization efficiency through functional polymer binders. Pan *et al.* and Yang *et al.* developed a self-healing binder containing polysulfide-confining groups (trithiocarbonate, carboxylic acids, and amino groups), which can not only effectively alleviate the pulverization of sulfur microparticles *via* the self-healing behavior, but also confine the migration of the generated polysulfide species.[30,31] Nevertheless, the small weight proportion of binders in cathodes cannot guarantee efficient adsorption or confinement of polysulfides. In this scenario, as proposed by Zhang and his colleagues, accelerating polysulfide conversion rather than blocking the dissolution and diffusion of polysulfides is a better strategy to suppress the shuttle effect.[21,32] Therefore, a polymer binder with polysulfide conversion accelerating ability would be effective in suppressing the shuttle effect even though its mass loading is small.

Based on the above consideration, we envisage that if a polymer binder with high flexibility, self-healing properties and polysulfide absorption/conversion ability can be designed, the overall performance of Li–S batteries can be improved. Herein, we developed a multifunctional self-healing polymer binder containing aromatic disulfide bonds (2S-PDMS). This polymer exhibits good adhesion and high stretchability, thus the resulting electrode can sustain the large volumetric changes of the sulfur electrode during lithiation/delithiation. Due to the dynamic nature of the aromatic disulfide bonds, this polymer also shows excellent self-healing behavior at room temperature. The self-healing process of the 2S-PDMS polymer can autonomously trigger damage repair during cycling (Fig. 1a). More importantly, the reversible breakage/formation of the S–S bond in 2S-PDMS molecules can not only capture polysulfides but also facilitate their conversion (Fig. 1a). As a result, 2S-PDMS-based sulfur cathodes exhibit excellent cycling performance, delivering a specific capacity of 545.7 mA h g^{-1} at 2.0C after 400 cycles. Additionally, soft-packed Li–S batteries with a higher loading of 6.6 mg cm^{-2} exhibit a fairly stable cycling performance with a high initial areal capacity of 7.53 mA h cm^{-2}.

Results and discussion

Design, synthesis and characterization of 2S-PDMS binders

Dynamic disulfide chemistry has been frequently used to derive novel functional materials, such as recyclable polymers, redox-reversible hydrogels and self-healing polymers.[33–36] It should be noted that the cleavage and reformation of aliphatic sulfide bonds have to be triggered by temperature or oxidants/reductants. Therefore, although disulfide bonds have been previously incorporated into polymer binders for Li–S batteries,[27,30,37] the dynamic exchange of disulfide bonds made little contribution to the improvement of the battery performance in these systems. According to the literature, disulfide bonds are dynamic at room temperature when they are linked to aromatic groups, thus leading to autonomous self-healing without external stimuli.[38,39] Therefore, we designed a self-healing polymer containing aromatic disulfide bonds for our study.

We synthesized the self-healing poly(dimethylsiloxane)-based (2S-PDMS) polymer by condensation reactions of bis(3-aminopropyl)-terminated poly(dimethylsiloxane) (H_2N-PDMS-NH_2, M_n = 700–900), 2,6-pyridinedicarbonyl dichloride and 4-aminophenyl disulfide (Fig. S1–S4†). Fig. 1b presents the molecular structure, in which the hydrogen bonds and S–S bonds of the 2S-PDMS polymer are highly dynamic. The 2S-PDMS polymer (2S to H_2N-PDMS-NH_2 molar ratio of 1 : 9) was selected as the optimal material (see the ESI† for the detailed

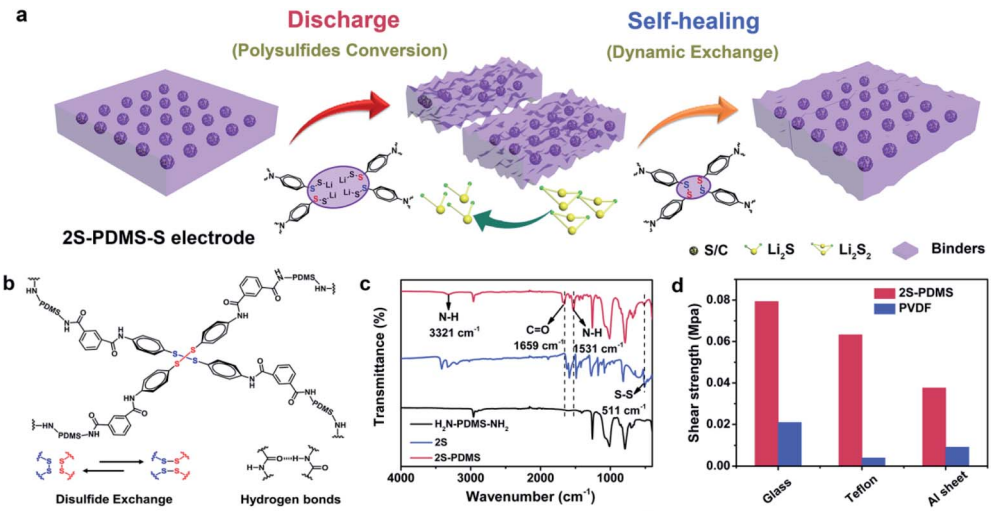

Fig. 1 Structural design of 2S-PDMS binders. (a) Illustration of the process of self-healing binders enabling cathode integrity and faster polysulfide conversion. Molecular structure (b) and the FT-IR spectrum (c) of the 2S-PDMS polymer. (d) Comparison of the shear strength between the 2S-PDMS polymer and commercial PVDF binder materials on glass, Teflon and Al sheet surfaces.

fabrication process). As shown in Fig. 1c, the Fourier transform-infrared (FT-IR) spectra indicate the characteristic peaks at 3321 cm^{-1} ν(N–H), 1659 cm^{-1} ν(C=O), 1531 cm^{-1} ν(amide II)[40] and 511 cm^{-1} ν(S–S).[41] Elemental mapping images (Fig. S5†) of the 2S-PDMS polymer show homogeneous distribution of the synthesized material. The obtained 2S-PDMS polymer exhibits good adhesion at room temperature. In comparison to the commercial PVDF binder, the 2S-PDMS polymer material shows enhanced adhesive forces on three tested surfaces (Fig. 1d, S6 and video S1†). The shear strength of the 2S-PDMS polymer is 0.080 MPa, which is much higher than that of the PVDF binder on glass surfaces. Its excellent adhesive properties are ascribed to the large number of hydrogen bonds formed between the amide bond of the 2S-PDMS polymer and the exposed atoms on the tested surface.[42,43]

Self-healing properties of 2S-PDMS binders

The 2S-PDMS polymer exhibits excellent self-healing properties. Fig. 2a shows that the scratch on the resulting polymer film almost disappeared after healing at room temperature for 8 hours. The polymer films were cut into two pieces and placed in contact with each other to allow self-healing. As shown in Fig. 2b, the tensile strength of the 2S-PDMS film is 0.033 MPa and recovers 82.5% of its pristine strength after healing for 30 min. The glass transition temperature (T_g) of the 2S-PDMS polymer network was measured to be approximately −50 °C (Fig. S7†), which is much lower than room temperature, indicating that the polymer chain has good fluidity at room temperature. The good dynamic properties of 2S-PDMS are also shown in the rheological measurements (Fig. S8†). Dynamic bonds can participate in interchange and rearrangement due to the excellent flowability of the polymer chain, thus facilitating the self-healing action of the material. The 2S-PDMS polymer not only exhibits self-healing capability but also has good flexibility and high stretchability at room temperature (Fig. S9 and S10†). The 2S-PDMS polymer can be processed into different shaped letters (such as “e”, “u”, “s” and “o” letters) and recycled through simple compression molding at room temperature. This feature highlights its excellent flexibility and processability. For the 2S-PDMS polymer, a maximum stretchability of 2280% can be achieved (Fig. S10†). In contrast, the strain of polyvinylidene fluoride (PVDF) before fracturing is merely 19%. Such remarkable self-healing ability, flexibility and adhesive properties are vital to binders. By mixing the 2S-PDMS polymer with conductive carbon (acetylene black, AB), we obtained a conductive composite which underwent electrical self-healing at room temperature (Fig. 2f). When the conductive film was cut and brought together, the light-emitting diode (LED) was relit after a few seconds, indicating good electrical self-healing capability. Next, we fabricated 2S-PDMS-S cathodes for lithium–sulfur batteries with 2S-PDMS polymers as a binders. PVDF-S electrodes were also fabricated as control samples.

The 2S-PDMS polymer has excellent self-healing properties, which are beneficial to the cycling stability of the 2S-PDMS-S electrode. To confirm this speculation, scanning electron microscopy (SEM) images of the electrodes with the two different binders before cycling are obtained and they show a homogeneous and flat morphology (Fig. S11†). After 5 cycles at a rate of C/10, cracks and voids appear on the surface of the PVDF-S electrode (Fig. 2c), causing reduced electrical conductivity and poor sulfur utilization. In comparison, the 2S-PDMS binder with a self-healing capability and excellent mechanical

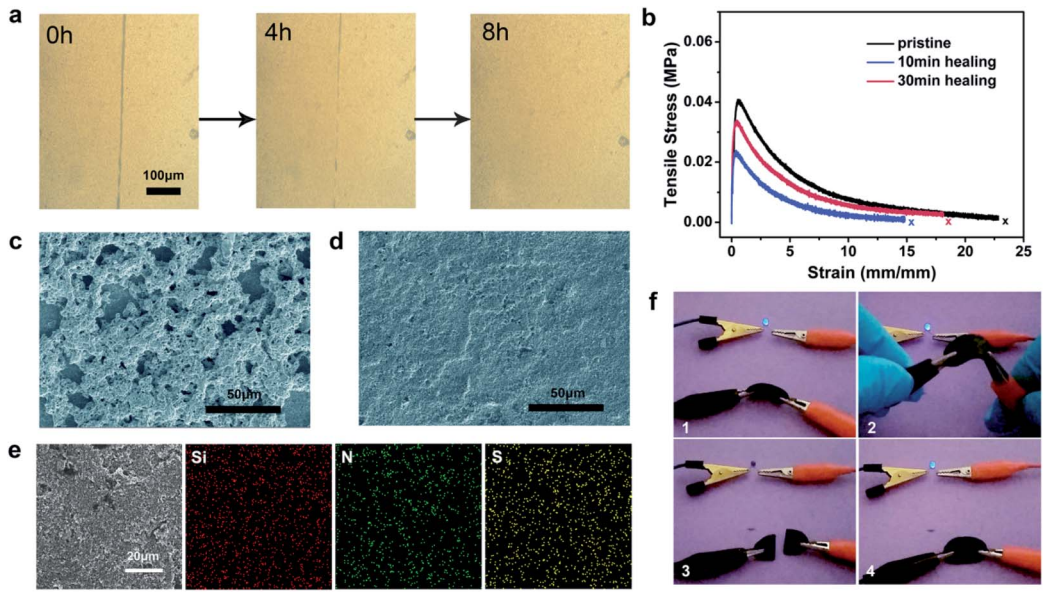

Fig. 2 Self-healing properties. (a) Optical microscope images of the damaged and healed 2S-PDMS polymer at room temperature in 0, 4, and 8 h, respectively. (b) Tensile tests of the 2S-PDMS polymer after different healing times. SEM images of sulfur cathodes with the PVDF polymer (c) and the 2S-PDMS polymer binder (d) after 5 cycles at a rate of C/10, respectively. (e) SEM image and elemental mapping images (Si, N, and S elements) of the 2S-PDMS-S electrode after cycling. (f) Optical images of the conductive composite with the 2S-PDMS binder that connects the LED devices before and after self-healing.

properties can integrate into the sulfur cathode without cracks and damage (Fig. 2d). After the cycling process, 2S-PDMS is evenly distributed on the electrode surface, while PVDF is randomly distributed on the surface because of electrode fracturing during cycling, as shown by elemental mapping (Fig. 2e and S12†). Consequently, this result suggests that the self-healing ability of 2S-PDMS can maintain the integrity of the sulfur cathode and reinforce electrode stability.

Electrochemical performance of Li–S batteries with the 2S-PDMS binder

A series of electrochemical tests were applied to show the accessibility of 2S-PDMS as an advanced binder material for Li–S batteries. Fig. 3a presents CV curves of the third scan for 2S-PDMS-S and PVDF-S electrodes at a scan rate of 0.1 mV s^{-1}. Obviously, the 2S-PDMS-S cathode exhibits two typical cathodic peaks (≈2.31 and 2.04 V) and one anodic peak (≈2.30–2.36 V) (Fig. S13†), corresponding to the multi-step reduction of S_8 and the conversion from Li_2S and/or Li_2S_2 to sulfur species.[44–46] The 2S-PDMS-S cathode delivers higher peak current densities, indicating larger sulfur utilization.

The cycling performances of 2S-PDMS-S and PVDF-S electrodes at 0.5C (with the first cycles cycled at 0.1C for activation; 1C = 1675 mA g^{-1}) are shown in Fig. 3b. Specifically, the specific capacity of the 2S-PDMS-S cathode is initially up to 1006.3 mA h g^{-1} and then sustains 763.6 mA h g^{-1} after 100 cycles. In contrast, the specific capacity of the PVDF-based electrode is 497.5 mA h g^{-1} after 100 cycles. The discharge/charge curves at 0.5C for the sulfur electrodes with the PVDF and 2S-PDMS binders are shown in Fig. 3c. The prolonged 1st plateaus and 2nd plateaus in the discharge–charge profiles of 2S-PDMS-S compared with those of PVDF-S show the higher utilization of active materials. Compared with PVDF electrodes, 2S-PDMS-S batteries show a smaller charge-transfer resistance of 33.73 Ω (Fig. 3d) due to better adhesion of the active material to the conductive agent as confirmed from SEM images (Fig. S11†), and hence polysulfide redox can take place easily on it. Generally, high-energy-density Li–S batteries with high-sulfur-content electrodes are critical for practical applications. When the sulfur content increases to 70 or 80% in S/C composites (Fig. S14 and S15†), batteries with the 2S-PDMS binder can deliver a higher capacity than those with the PVDF binder.

The rate performances of sulfur electrodes with the PVDF and 2S-PDMS binders at various current densities are shown in Fig. 3e. The specific capacities of the 2S-PDMS-S cathode are much higher than those of the PVDF-S cathode. In detail, at 0.2C, a high initial capacity of 1241.3 mA h g^{-1} is obtained for the 2S-PDMS-S cathode. Moreover, the 2S-PDMS-S cathode delivers a high reversible discharge capacity of 824.2, 706.5, 629.4 and 546.0 mA h g^{-1} at 0.5, 1, 2 and 4C, respectively. The corresponding galvanostatic charge–discharge profiles of the sulfur electrodes with PVDF and 2S-PDMS binders are shown in Fig. 3f and S16.† As the current rate increases from 0.2C to 4.0C,

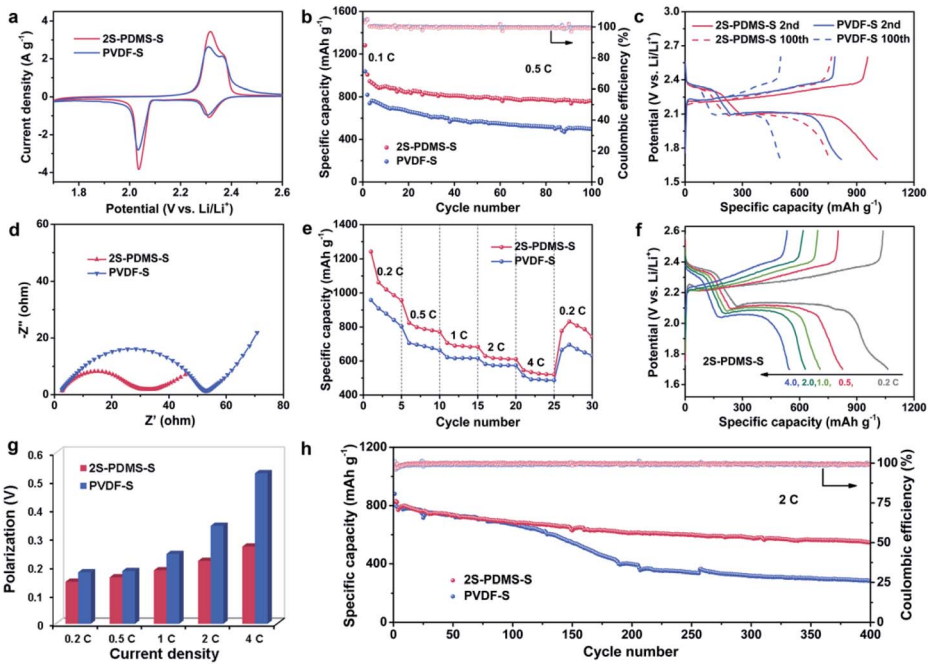

Fig. 3 Electrochemical performance of the 2S-PDMS-S electrode. (a) CV curves of the third scan for 2S-PDMS-S and PVDF-S electrodes at a scan rate of 0.1 mV s^{-1}. (b) Cycling performances of 2S-PDMS-S and PVDF-S electrodes at 0.5C (with the first cycles cycled at 0.1C for activation) and the (c) corresponding galvanostatic charge–discharge profiles. (d) The Nyquist plot of sulfur electrodes with two different polymer binders. (e) Rate capabilities of sulfur electrodes with 2S-PDMS and PVDF binders at various current densities from 0.2 to 4C and the (f) corresponding galvanostatic charge–discharge profiles of 2S-PDMS-S electrodes. (g) The column chart of the polarization values in galvanostatic charge–discharge curves for 2S-PDMS-S and PVDF-S electrodes. (h) Long-term cycling performance of sulfur electrodes with 2S-PDMS and PVDF binders at 2C.

the discharge curve of the 2S-PDMS-based electrode exhibits stable plateaus with lower polarization values (Fig. 3g), indicating its superior rate capability with faster redox kinetics. In contrast, the voltage hysteresis remarkably increases at high rates for the PVDF-based electrodes. This distinction can also be explained by the large charge transfer resistance of the PVDF-based electrode (Fig. 3d).

Fig. 3h shows the long-term cycling performance at 2C. After 100 cycles, the capacity of PVDF-S drastically faded. The fading rate is up to 0.193% per cycle over 300 cycles, calculated from the 100th cycle to 400th cycle, indicating that the severe volume variation of sulfur species in the cathodes destroys the integrity of the PVDF-S cathodes. 2S-PDMS polymers with excellent self-healing ability and flexibility as binders can remarkably improve the cycling performance. The 2S-PDMS-S cathode at 2.0C reaches 545.7 mA h g^{-1} with a capacity decay of only 0.068% per cycle after 400 cycles and coulombic efficiencies close to 100%, implying stable cycling performance. When cycled at current densities of 1C (Fig. S17†), the 2S-PDMS-S cathode also shows higher sulfur utilization and better cycling stability. The 2S-PDMS-S electrode has excellent cycling performance due to the self-healing behavior of the 2S-PDMS polymer.

Mechanism exploration

Electrochemical measurement results demonstrate the superiority of 2S-PDMS as a binder for Li–S batteries. To verify the influence of 2S-PDMS, we performed a series of control experiments. As shown in Fig. S18,† the specific capacity of the PDMS-S electrodes (PDMS indicates polymer without the disulfide unit) is close to that of the PVDF-S electrode. In addition, the introduction of a certain amount of the 2S compound in the 2S-PDMS polymer can effectively enhance the specific capacity (Fig. S18–S21†). To further confirm the effect of the S–S bonds on the 2S-PDMS binder, 2S-PDMS/AB electrodes were prepared with acetylene black and the 2S-PDMS binder (1 : 1 in weight). The specific capacity of the 2S-PDMS/AB electrode is only 3 mA h g^{-1} at 100 mA g^{-1}, indicating that the improved capacity is not due to the contribution of 2S-PDMS (Fig. S22†). The CV curve of the 2S-PDMS/AB electrode shows one cathodic peak (≈2.03 V) and one anodic peak (≈2.48 V), which can be attributed to the fracture and formation of the S–S bond in the 2S-PDMS polymer, respectively.[47] *Ex situ* X-ray photoelectron spectroscopy (XPS) spectra of the 2S-PDMS-S electrode before and after the 5th cycle in the fully discharged or fully charged state are shown in Fig. 4a–c. For the pristine 2S-PDMS-S electrode, the S 2p spectrum can be deconvoluted into the C–S peak at 164.2 eV and two peaks for S–S at 163.5 and 164.9 eV.[47,48] The existence of a strong peak for the C–S component indicates a strong interaction of 2S-PDMS with sulfur in the S/C composites. In the refined S 2p spectrum of discharged batteries, there are two peaks at 160.0 and 160.8 eV attributed to the final discharge product Li_2S[27,49] and a peak corresponding to short-chain lithium organosulfides (C–S–Li^+) at 161.6 eV.[27] The peak of the incomplete discharge product (Li_2S_2) at 162.0 eV[27] is not observed, suggesting the relatively complete conversion of sulfur to Li_2S or C–S–Li^+. In the spectra of the fully charged batteries, in addition to some Li_2S and lithium salt residues in the cathodes restricted in the pores of carbon, there are peaks for S–S and C–S, demonstrating the reversible electrochemical

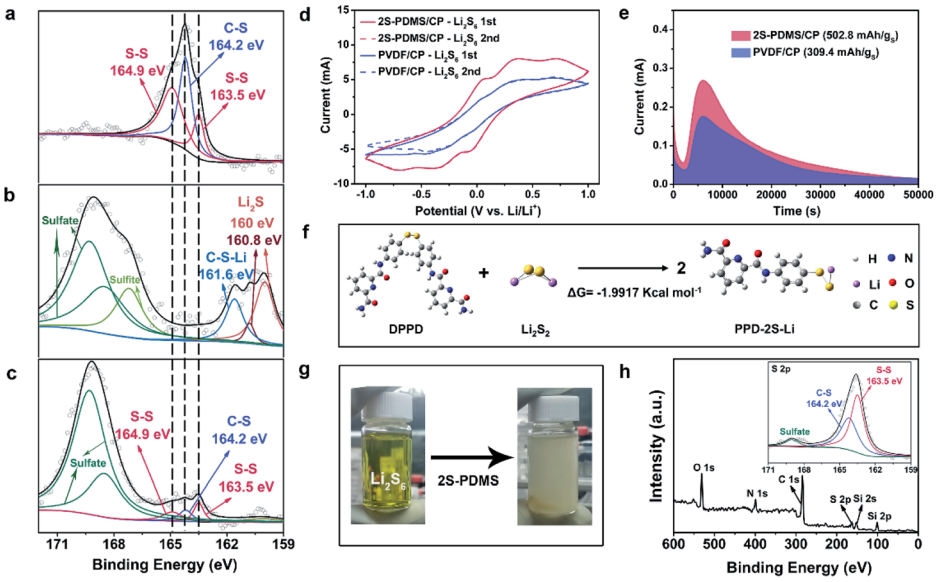

Fig. 4 Polysulfide conversion mechanism of the 2S-PDMS-S electrode. High-resolution S 2p XPS spectra of the 2S-PDMS-S electrode before (a) and after the 5th cycle in fully-discharged (b) or fully-charged states (c). (d) CV curves of the Li_2S_6 symmetric batteries conducted on two identical PVDF/CP or 2S-PDMS/CP electrodes (e) potentiostatic discharge profiles at 2.04 V for evaluating the kinetics of Li_2S deposition on PVDF/CP or 2S-PDMS/CP. (f) Gibbs free energy of the polysulfide conversion reaction acquired from quantum chemistry calculations. (g) Digital images of the polysulfide conversion process after introducing 2S-PDMS binders. (h) XPS spectrum and the corresponding refined S 2p spectrum of the 2S-PDMS binder after interacting with the polysulfide solution.

conversion of sulfur and short-chain polysulfides in the 2S-PDMS-S cathodes. XPS tests and CV curves of 2S-PDMS/AB proved that the disulfide bonds in 2S-PDMS molecules can reversibly break and reform during charge–discharge cycling to generate short-chain lithium organosulfides and hence accelerate the conversion of polysulfides.

To further demonstrate the ability of 2S-PDMS to accelerate polysulfide conversion, typical Li_2S_6 symmetric cell tests and potentiostatic Li_2S deposition tests developed by Zhang *et al.* and Chiang *et al.* were conducted.[21,50] These two powerful methods can be used to evaluate the rate of polysulfide conversion kinetics in the liquid phase and Li_2S deposition kinetics, respectively. In Fig. 4d, Li_2S_6 symmetric cells were assembled on PVDF/carbon paper(CP) and 2S-PDMS/CP, for both of which CV curves were acquired at a scan rate of 3 mV s^{-1}. It is obvious that the reversible current density of 2S-PDMS/CP is always higher than that of PVDF/CP. Additionally, more clarified redox peaks corresponding to Li_2S_8/Li_2S_6, Li_2S_6/Li_2S_4 and Li_2S_4/Li_2S at 0.064/-0.063, 0.36/-0.358 and 0.71/-0.71 V are also shown in curves of 2S-PDMS/CP.[51] In contrast, the current density of PVDF/CP decreases with the increasing cycle number, and there are always ambiguous redox peaks. These results indicate that 2S-PDMS can afford enhanced polysulfide conversion kinetics compared with commercial PVDF binders. The kinetics of lithium sulfide deposition on these two substrates were also estimated. In a classical potentiostatic discharge test (Fig. S23†), the current falls down at the initial stage, corresponding to Li_2S_8 reduction, which will further take part in background current contribution. Then, the current will rise to a peak value again, and fade until below 0.01 mA gradually. After subtracting the background current, the bump area corresponds to the electric quantity of the Faraday process of Li_2S deposition.[50] It can be observed that the amount of electric quantity of Li_2S deposition on 2S-PDMS/CP is larger than that of PVDF/CP, further proving the superior ability of 2S-PDMS to accelerate polysulfide conversion (Fig. 4e).

To understand the possible mechanism at the molecular level of 2S-PDMS accelerating polysulfide conversion kinetics, density functional theory (DFT) calculations of the reactions between 2S-PDMS molecules and polysulfides were performed with the Gaussian 09 package.[52] Fig. 4f shows the model molecular structures of N^2,$N^{2\prime}$-(disulfanediylbis(4,1-phenylene)) bis(pyridine-2,6-dicarboxamide) (DPPD, for short) and its derivates and polysulfides using GaussianView software.[53] The Gibbs free energy (ΔG) of the reaction of the DPPD molecule with Li_2S_2 to form PPD-2S-Li (*N*-phenylpyridine-2,6-dicarboxamide, PPD) is calculated to be -1.9917 Kcal mol^{-1} (Fig. S24, S25, Tables S1 and S2†), indicating the spontaneous trend of DPPD capturing Li_2S_2 through disulfide bonds, as reported in previous studies.[54] It should be noted that although the Gibbs free energy of the reaction between PVDF and Li_2S_2 is a negative value (Fig. S26†), the mechanism of the 2S-PDMS binder interacting with Li_2S_2 is totally different from that of PVDF. The former is a chemical conversion reaction while the latter is just an adsorption process. In addition, the formed PPD-2S-Li/PPD-3S-Li can further couple the conversion reaction from Li_2S_8 to Li_2S_6 with the reaction $\Delta G < 0$, enabling reversible and highly efficient redox in Li–S batteries. Lithium organosulfides can be converted to Li_2S more easily than insulating Li_2S_2.[27] Therefore, the polysulfides generated during charge/discharge processes can be quickly converted to the final discharge product Li_2S in cathodes. In this way, the shuttling effect can be significantly suppressed in spite of the small quantity of the binder. Such a strategy to accelerate polysulfide conversion rather than blocking their diffusion, as inspired by the Chinese legend of 'Emperor Yu tames the flood', has also been proved to be efficient in a previous study.[21,32,55–57]

To observe the process of 2S-PDMS converting the polysulfide more intuitively digital images of a Li_2S_6 solution(10 mM in DME) before and after adding 10 mg 2S-PDMS were collected (Fig. 4g). Before addition, the solution shows a transparent light yellow color. After adding the 2S-PDMS binder and slightly shaking, the solution changed into a milk-white suspension, suggesting the formation of short-chain polysulfides.[58] Insoluble suspended solids were gathered by centrifugation in a Ar-filled glove-box and subjected to XPS characterization after 50 °C heating on a hotplate until the solvent completely volatilized. The XPS spectrum (Fig. 4h) of these solids indicates there are Si, N, C, and O elements originating from 2S-PDMS, and additionally there is also a strong S 2p signal which can be only from the polysulfides in the solution (Fig. S27†). The refined S 2p spectrum also points out the existence of both S–S and C–S species and some sulfate from polysufide oxidation, affirming the capture of polysulfides by 2S-PDMS.

Application of 2S-PDMS in soft-packed Li–S batteries

The 2S-PDMS binders can also be applied in soft-packed Li–S batteries due to good flexibility and stability of the PDMS

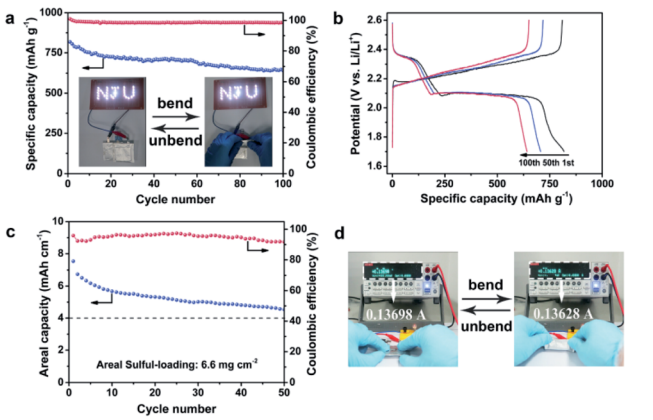

Fig. 5 Electrochemical performance of soft-packed Li–S batteries. Cycling performance (a) and galvanostatic discharge–charge profiles (b) of 2S-PDMS-S (loading 2.2 mg_s cm^{-2}, size: 3 cm × 4 cm) soft-packed Li–S batteries. Inset: optical images of soft-packed batteries lighting up LED devices with the pattern of "NJU" under continuous bending-unbending operations. (c) The cycling stability of 2S-PDMS-S (size: 3 cm × 4 cm) soft-packed batteries with a sulfur loading of 6.6 mg_s cm^{-2} at 0.42 mA cm^{-2}. (d) 2S-PDMS-S soft-packed Li–S batteries connected to a Keithley 2400 in order to monitor current changes in the circuit before and after the bending test.

backbone. For low-loading soft-packed batteries, the use of this binder results in an initial discharge capacity of 817.8 mA h g^{-1}, and the discharge capacity remains at 641.6 mA h g^{-1} after 100 cycles (Fig. 5a). As depicted in Fig. 4b, the two typical plateaus in the galvanostatic discharge–charge profiles from the 1st to 100th cycles show little capacity decay and no obvious increase in voltage hysteresis. When increasing to a higher loading of 6.6 mg cm^{-2} (Fig. 5c), the soft-packed Li–S batteries deliver a fairly stable cycling performance from an initial areal capacity of 7.53 mA h cm^{-2} and still retain an areal capacity of 4.54 mA h cm^{-2} after 50 cycles, surpassing commercial Li-ion batteries (4 mA h cm^{-2}).[59] Encouragingly, an LED lamp, electronic hygrothermograph and a series of LED devices with the pattern of "NJU" were lit by soft-packed Li–S batteries to establish their practical applications (Fig. S28b,† Fig. 5a and video S2†). To further demonstrate the safety and flexibility requirements, the brightness of LED devices with the pattern of "NJU" under continuous bending-unbending operations was monitored and showed no obvious change (Fig. 5a and video S2†). Moreover, a Keithley 2400 instrument was used to monitor current and voltage changes in the circuit. Through two kinds of circuit connections (Fig. S29†), we further observed that the current and voltage are almost constant ($I \approx 0.13698$ A and $V \approx 2.1650$ V) under continuous bending–unbending operations of soft-packed Li–S batteries (Fig. 5d, S29, S30 and video S3†), verifying their good flexibility and stability.

Conclusions

In summary, we successfully prepared a self-healing poly(dimethylsiloxane)-based polymer as a binder for application in lithium–sulfur batteries. The 2S-PDMS binder with excellent adhesive properties can effectively connect active materials together with conductivity additives and accelerate charge transfer in cathodes. The exchange of dynamic bonds (hydrogen bonds and S–S bonds) in the 2S-PDMS polymer results in good flexibility, high stretchability and a remarkable self-healing ability, assisting in repairing damage caused by electrode volume variations and integration in sulfur cathodes. More importantly, *ex situ* XPS spectra, electrochemical tests and DFT calculations confirmed that the reversible breakage/formation of the S–S bonds in 2S-PDMS molecules can help to capture polysulfides and accelerate their conversion. Benefiting from these merits, 2S-PDMS-S electrodes exhibited outstanding rates and cycling performances. In particular, soft-packed Li–S batteries with a high loading of 6.6 mg cm^{-2} delivered decent cycling stability with a high areal capacity of 7.53 mA h cm^{-2}. The strategy of improving the performance of Li–S batteries through multifunctional polymer binders can be potentially generalized for other lithium ion batteries.

Conflicts of interest

There are no conflicts to declare.

Acknowledgements

This work was supported by the National Natural Science Foundation of China (Grant No. 21631006 and 21771100), the Natural Science Foundation of Jiangsu Province (Grant No. BK20170016), and the Scientific Research Foundation of Graduate School of Nanjing University (2018CL04).

Notes and references

1 X. Ji and L. F. Nazar, *J. Mater. Chem.*, 2010, **20**, 9821.
2 M. Wild, L. O'Neill, T. Zhang, R. Purkayastha, G. Minton, M. Marinescu and G. J. Offer, *Energy Environ. Sci.*, 2015, **8**, 3477.
3 Q. Pang, X. Liang, C. Y. Kwok and L. F. Nazar, *Nat. Energy*, 2016, **1**, 16132.
4 H. J. Peng, J. Q. Huang, X. B. Cheng and Q. Zhang, *Adv. Energy Mater.*, 2017, **7**, 1770141.
5 H. Yuan, J. Q. Huang, H. J. Peng, M. M. Titirici, R. Xiang, R. Chen, Q. Liu and Q. Zhang, *Adv. Energy Mater.*, 2018, **8**, 1802107.
6 X. Ji, K. T. Lee and L. F. Nazar, *Nat. Mater.*, 2009, **8**, 500.
7 J. Schuster, G. He, B. Mandlmeier, T. Yim, K. T. Lee, T. Bein and L. F. Nazar, *Angew. Chem., Int. Ed.*, 2012, **51**, 3591.
8 W. Ai, W. Zhou, Z. Du, Y. Chen, Z. Sun, C. Wu, C. Zou, C. Li, W. Huang and T. Yu, *Energy Storage Materials*, 2017, **6**, 112.
9 J. Liu, W. Li, L. Duan, X. Li, L. Ji, Z. Geng, K. Huang, L. Lu, L. Zhou, Z. Liu, W. Chen, L. Liu, S. Feng and Y. Zhang, *Nano Lett.*, 2015, **15**, 5137.
10 G. Zhou, E. Paek, G. S. Hwang and A. Manthiram, *Nat. Commun.*, 2015, **6**, 7760.
11 J. Song, Z. Yu, M. L. Gordin and D. Wang, *Nano Lett.*, 2016, **16**, 864.
12 W. Zhou, Y. Yu, H. Chen, F. J. DiSalvo and H. D. Abruña, *J. Am. Chem. Soc.*, 2013, **135**, 16736.
13 J. Wang, J. Yang, J. Xie and N. Xu, *Adv. Mater.*, 2002, **14**, 963.
14 L. Ma, R. Chen, G. Zhu, Y. Hu, Y. Wang, T. Chen, J. Liu and Z. Jin, *ACS Nano*, 2017, **11**, 7274.
15 Z. W. Seh, W. Li, J. J. Cha, G. Zheng, Y. Yang, M. T. McDowell, P.-C. Hsu and Y. Cui, *Nat. Commun.*, 2013, **4**, 1331.
16 G. Li, W. Lei, D. Luo, Y. P. Deng, D. Wang and Z. Chen, *Adv. Energy Mater.*, 2018, **8**, 1702381.
17 S. Evers, T. Yim and L. F. Nazar, *J. Phys. Chem. C*, 2012, **116**, 19653.
18 L. Li, L. Chen, S. Mukherjee, J. Gao, H. Sun, Z. Liu, X. Ma, T. Gupta, C. V. Singh, W. Ren, H. M. Cheng and N. Koratkar, *Adv. Mater.*, 2017, **29**, 1602734.
19 J. He, Y. Chen and A. Manthiram, *Energy Environ. Sci.*, 2018, **11**, 2560.
20 L. Fan, M. Li, X. Li, W. Xiao, Z. Chen and J. Lu, *Joule*, 2019, **3**, 361.
21 Z. Yuan, H. J. Peng, T. Z. Hou, J. Q. Huang, C. M. Chen, D. W. Wang, X. B. Cheng, F. Wei and Q. Zhang, *Nano Lett.*, 2016, **16**, 519.
22 A. Vizintin, R. Guterman, J. Schmidt, M. Antonietti and R. Dominko, *Chem. Mater.*, 2018, **30**, 5444.

23 B. Koo, H. Kim, Y. Cho, K. T. Lee, N. S. Choi and J. Cho, *Angew. Chem., Int. Ed.*, 2012, **51**, 8762.
24 J. Pan, G. Xu, B. Ding, J. Han, H. Dou and X. Zhang, *RSC Adv.*, 2015, **5**, 13709.
25 W. Bao, Z. Zhang, Y. Gan, X. Wang and J. Lia, *J. Energy Chem.*, 2013, **22**, 790.
26 X. Hong, J. Jin, Z. Wen, S. Zhang, Q. Wang, C. Shen and K. Rui, *J. Power Sources*, 2016, **324**, 455.
27 F. L. Zeng, N. Li, Y. Q. Shen, X. Y. Zhou, Z. Q. Jin, N. Y. Yuan, J. N. Ding, A. B. Wang, W. K. Wang and Y. S. Yang, *Energy Storage Materials*, 2019, **18**, 190.
28 L. Li, T. A. Pascal, J. G. Connell, F. Y. Fan, S. M. Meckler, L. Ma, Y.-M. Chiang, D. Prendergast and B. A. Helms, *Nat. Commun.*, 2017, **8**, 2277.
29 Z. Chang, Y. He, H. Deng, X. Li, S. Wu, Y. Qiao, P. Wang and H. Zhou, *Adv. Funct. Mater.*, 2018, **28**, 1804777.
30 Y. Chu, X. Cui and Q. Pan, *ACS Appl. Energy Mater.*, 2018, **1**, 6919.
31 Z. Yu, T. Gao, T. Le, W. Wang, L. Wang and Y. Yang, *J. Mater. Sci.: Mater. Electron.*, 2019, **30**, 5536.
32 R. Xu, J. Q. Huang and Q. Zhang, *Matter*, 2019, **1**, 300.
33 G. C. Tesoro and V. Sastri, *J. Appl. Polym. Sci.*, 1990, **39**, 1425.
34 V. R. Sastri and G. C. Tesoro, *J. Appl. Polym. Sci.*, 1990, **39**, 1439.
35 Y. Chujo, K. Sada, A. Naka, R. Nomura and T. Saegusa, *Macromolecules*, 1993, **26**, 883.
36 J. Canadell, H. Goossens and B. Klumperman, *Macromolecules*, 2011, **44**, 2536.
37 C. Q. Niu, J. Liu, T. Qian, X. W. Shen, J. Q. Zhou and C. L. Yan, *Natl. Sci. Rev.*, 2020, **7**, 315.
38 A. Rekondo, R. Martin, A. Ruiz de Luzuriaga, G. Cabañero, H. J. Grande and I. Odriozola, *Mater. Horiz.*, 2014, **1**, 237.
39 I. Azcune and I. Odriozola, *Eur. Polym. J.*, 2016, **84**, 147.
40 C. H. Li, C. Wang, C. Keplinger, J. L. Zuo, L. Jin, Y. Sun, P. Zheng, Y. Cao, F. Lissel and C. Linder, *Nat. Chem.*, 2016, **8**, 618.
41 Y. Zhang, Y. Peng, Y. Wang, J. Li, H. Li, J. Zeng, J. Wang, B. J. Hwang and J. Zhao, *Sci. Rep.*, 2017, **7**, 11386.
42 A. H. Hofman, I. A. van Hees, J. Yang and M. Kamperman, *Adv. Mater.*, 2018, **30**, 1704640.
43 B. Coupe, M. E. Evangelista, R. M. Yeung and W. Chen, *Langmuir*, 2001, **17**, 1956.
44 X. Liang, M. Zhang, M. R. Kaiser, X. Gao, K. Konstantinov, R. Tandiono, Z. Wang, H. K. Liu, S. X. Dou and J. Wang, *Nano Energy*, 2015, **11**, 587.
45 G. Zhou, Y. Zhao and A. Manthiram, *Adv. Energy Mater.*, 2015, **5**, 1402263.
46 W. Zhou, C. Wang, Q. Zhang, H. D. Abruña, Y. He, J. Wang, S. X. Mao and X. Xiao, *Adv. Energy Mater.*, 2015, **5**, 1401752.
47 X. Liu, A. Wang, S. Wang, X. Liu, J. Chen, H. Xu, Q. Zeng and L. Zhang, *J. Electrochem. Soc.*, 2018, **165**, A1297.
48 W. Wang, Z. Cao, G. A. Elia, Y. Wu, W. Wahyudi, E. Abou-Hamad, A. H. Emwas, L. Cavallo, L. J. Li and J. Ming, *ACS Energy Lett.*, 2018, **3**, 2899.
49 X. Liang, C. Hart, Q. Pang, A. Garsuch, T. Weiss and L. F. Nazar, *Nat. Commun.*, 2015, **6**, 5682.
50 F. Y. Fan, W. C. Carter and Y. M. Chiang, *Adv. Mater.*, 2015, **27**, 5203.
51 M. Yu, S. Zhou, Z. Wang, W. Pei, X. Liu, C. Liu, C. Yan, X. Meng, S. Wang, J. Zhao and J. Qiu, *Adv. Funct. Mater.*, 2019, **29**, 1905986.
52 M. J. Frisch, G. W. Trucks, H. B. Schlegel, G. E. Scuseria, M. A. Robb, J. R. Cheeseman, G. Scalmani, V. Barone, B. Mennucci, G. A. Petersson, H. Nakatsuji, M. Caricato, X. Li, H. P. Hratchian, A. F. Izmaylov, J. Bloino, G. Zheng, J. L. Sonnenberg, M. Hada, M. Ehara, K. Toyota, R. Fukuda, J. Hasegawa, M. Ishida, T. Nakajima, Y. Honda, O. Kitao, H. Nakai, T. Vreven, J. A. Montgomery Jr, J. E. Peralta, F. Ogliaro, M. Bearpark, J. J. Heyd, E. Brothers, K. N. Kudin, V. N. Staroverov, R. Kobayashi, J. Normand, K. Raghavachari, A. Rendell, J. C. Burant, S. S. Iyengar, J. Tomasi, M. Cossi, N. Rega, J. M. Millam, M. Klene, J. E. Knox, J. B. Cross, V. Bakken, C. Adamo, J. Jaramillo, R. Gomperts, R. E. Stratmann, O. Yazyev, A. J. Austin, R. Cammi, C. Pomelli, J. W. Ochterski, R. L. Martin, K. Morokuma, V. G. Zakrzewski, G. A. Voth, P. Salvador, J. J. Dannenberg, S. Dapprich, A. D. Daniels, Ö. Farkas, J. B. Foresman, J. V. Ortiz, J. Cioslowski and D. J. Fox, *Gaussian 09, Revision B.01*, Gaussian, Inc., Wallingford CT, 2010.
53 R. Dennington, T. Keith and J. Millam, *GaussView, Version 5*, Semichem Inc., Shawnee Mission KS, 2009.
54 W. Hua, Z. Yang, H. Nie, Z. Li, J. Yang, Z. Guo, C. Ruan, X. a. Chen and S. Huang, *ACS Nano*, 2017, **11**, 2209.
55 W. Chen, T. Lei, T. Qian, W. Lv, W. He, C. Wu, X. Liu, J. Liu, B. Chen, C. Yan and J. Xiong, *Adv. Energy Mater.*, 2018, **8**, 1702889.
56 G. Zhou, K. Liu, Y. Fan, M. Yuan, B. Liu, W. Liu, F. Shi, Y. Liu, W. Chen, J. Lopez, D. Zhuo, J. Zhao, Y. Tsao, X. Huang, Q. Zhang and Y. Cui, *ACS Cent. Sci.*, 2018, **4**, 260.
57 H. Yi, T. Lan, Y. Yang, Z. Lei, H. Zeng, T. Tang, C. Wang and Y. Deng, *J. Mater. Chem. A*, 2018, **6**, 18660.
58 C. Z. Zhao, X. B. Cheng, R. Zhang, H. J. Peng, J. Q. Huang, R. Ran, Z. H. Huang, F. Wei and Q. Zhang, *Energy Storage Materials*, 2016, **3**, 77.
59 H.-J. Peng, J.-Q. Huang, X.-B. Cheng and Q. Zhang, *Adv. Energy Mater.*, 2017, **7**, 1700260.